KSME

Springer

Journal of Mechanical Science and Technology 34 (2) 2020

Original Article
DOI 10.1007/s12206-020-0139-y

Keywords:
· Engine friction
· Strip-down method
· Friction model
· Piston
· Journal bearing

Correspondence to:
Sungwook Park
parks@hanyang.ac.kr

Citation:
Lee, S., Kang, J., Park, S. (2020). Measurement and modeling of crank train friction in light-duty diesel engines. Journal of Mechanical Science and Technology 34 (2) (2020) 889~903.
http://doi.org/10.1007/s12206-020-0139-y

Received May 1st, 2019
Revised December 1st, 2019
Accepted December 26th, 2019

† Recommended by Editor
Yong Tae Kang

Measurement and modeling of crank train friction in light-duty diesel engines

Seokhwon Lee[1], Jongdae Kang[1] and Sungwook Park[2]

[1]Department of Mechanical Convergence Engineering, Graduate School, Hanyang University, Seoul 04763, Korea, [2]School of Mechanical Engineering, Hanyang University, Seoul 04763, Korea

Abstract In this study, we present measurements and calculations of friction energy loss in the crank train of a light-duty vehicle diesel engine. The main objectives are to estimate the friction loss of each engine component and demonstrate the validity of our MATLAB-based friction modeling method. Friction measurement results obtained through a strip-down method are utilized to separate the entirety of engine friction loss into individual components group. The results from measurements and calculations are compared to verify our friction model. The model considers the lubrication for crank train components through the solution of Reynolds equations. Our friction modeling method is used to analyze the friction characteristics of piston rings, skirts, and main journal bearings with engine load variation. The numerical results show that the friction loss is increased under the high load condition because the contact friction is occurred due to the effect of reduced oil thickness. The experimental results for the variant temperature of the oil and coolant show that lower oil temperature increases the oil viscosity, so it affects the friction increasing.

1. Introduction

Automotive manufacturers are developing high-efficiency engines to meet strict emission regulations. Since the thermodynamic work performed by the engine is subject to thermal and mechanical energy losses, it is important to reduce energy losses to improve internal combustion engine efficiency [1]. There are many strategies for reducing energy loss in internal combustion engines, including novel combustion technology such as homogeneous charge compression-ignition (HCCI), various fuel injection strategies, waste heat recovery, engine downsizing, cylinder deactivation, and variable oil pumps.

In the internal combustion engine, friction occurs in many components, including piston assembly, crankshaft, connecting rods, valves, and auxiliary devices [2]. There are various friction reduction technologies, including surface coatings and textures that are used to reduce the friction coefficient, component geometry optimization which includes reduction of the bearing diameter and width and ring tension changes, component weight reduction, and lubrication condition changes such as the use of solid lubricant and low-viscosity oil. Recent experimental and modeling research on surface texturing has focused on the reduction of friction between contact surfaces. Zhou et al. [3] developed a theoretical model of load carrying capacity and film thickness using an optimal texturing design method. Usman and Park [4] optimized the textured barrel-shaped piston ring and surface texture pattern for reduced frictional losses in an SI engine. To develop the engine friction reduction technologies and verify availability, it is necessary to perform friction loss estimation for each engine component, and it is important to accurately measure and calculate engine friction loss.

Measuring engine friction is challenging. In terms of the total energy generated from the fuel, the contribution of the engine friction loss is small [5]. When compared to the energy transferred to the transmission, the contribution increases slightly. The accuracy of the engine friction measurements is very important [6]. Generally, the total engine friction, called FMEP, is estimated by determining the difference between IMEP, obtained from measuring cylinder

pressure, and BMEP, obtained from measuring engine transmission brake torque. However, there is a strong possibility for error when using this method because IMEP and BMEP are both much larger than FMEP [6].

There are four main estimation methods for determining engine friction: component removal, difference testing, direct measurement, and analytical modeling [5]. A strip-down method is the experimental method based on component removal to measure the friction of each part. The friction for each engine component is determined by measuring the difference in engine motoring torque before and after removing the component [7]. In the case of the combustion conditions, it is not possible to measure the friction of each engine component without engine alteration. For example, a floating liner device, made from a single-cylinder engine, is used to measure the piston assembly friction force [8]. Generally, the cylinder block floats, so it is important to seal the combustion gas pressure for accurate piston friction measurement. In this condition, a precise piston friction measurement is extremely time consuming and costly. Furthermore, the IMEP method is used to measure piston assembly friction under the fired engine condition [9]. In this method, a special grasshopper linkage was used to measure the connecting rod force. The piston assembly force is determined indirectly from the balance of the piston assembly friction force, the force acting on the piston assembly, the force acting on the connecting rod, the piston assembly axial acceleration, and the gas force.

The friction for each engine component can be measured under motored engine conditions without engine alteration. The contribution of each component friction to the whole engine friction is analyzed through a strip-down method. The drawback of this method is that it cannot reflect the actual deformation of each component in the fired engine condition [10]. To compensate for this drawback and to accurately research the engine friction, a combination of measurement and simulation is required. Therefore, the calculation for determining crank train friction was conducted at various engine operating conditions.

Numerical analysis of the engine part friction loss has occurred for decades. For the friction analysis of piston skirt, equations for oil lubrication and piston skirt behavior were considered in previous studies [11-13]. Zhu et al. [11] presented basic modeling in mixed lubrication. Livanos et al. [12] derived the dynamic equation, including the friction force of the piston ring. Meng et al. [13] suggested a dynamic equation to consider the inertia of the connecting rod. The lubrication equation is based on the Reynolds equation and is used to calculate the oil pressure at the piston skirt. To reflect the actual physical phenomena, it is necessary to add the roughness and waviness values of the materials to the Reynolds equation. Patir and Cheng [14, 15] used an average Reynolds equation, including roughness and flow factors, and the average Reynolds equation was used in this study.

The cylinder gas flow model, the force equilibrium equation, and the Reynolds equation were used in the friction analysis of the piston rings. Kuo et al. [16] predicted the flow of piston-ring crevices and orifices. Yun [17] suggested a numerical analysis method for determining the gas flow in the piston ring pack. Chong et al. [18] modeled the friction performance of an internal combustion engine. Lyubarskyy and Bartel [19] used a 2D CFD-model to analyze piston ring dynamics, mass transport, and friction. Jeng et al. [20, 21] proposed boundary conditions for varying amounts of lubricant. Han et al. [22] suggested a new boundary condition for the lubricant pressure to solve the 1D Reynolds equation. Choi et al. [23] describe a numerical simulation of the first compression piston ring in a diesel engine. Zhou et al. [24] developed a coupled method based on the heat transfer, the oil lubricant, and the friction of the piston-cylinder.

For the friction analysis of journal bearings, it is necessary to solve the Reynolds equation by considering the forces applied to the journal bearing from a connecting rod driven by combustion. Booker [25] presented a mobility method to easily conduct the bearing lubricant analysis. Hirani et al. [26] suggested an analytical method based on the model by Booker. Mourelatos et al. [27] proposed a finite element method for journal bearing hydrodynamic analysis.

The focus of this study is to investigate the friction characteristics of detailed components taking into account changes in engine load, oil and coolant temperature. Therefore, this study quantified the correlation between engine friction measurement and calculation. The strip-down method was used to measure the FMEP of each component group for the crank train and to analyze the contribution for each component group in the total engine friction loss. The result for measurement was used to validate the developed friction models. In the calculation process for modeling, the lubricant oil film pressure and thickness were calculated to determine the friction force and the power loss of each crank train component, such as the piston ring, the piston skirt, and the main journal bearing. The numerical analysis is based on the Reynolds equation and the dynamic equation. The Reynolds equation is calculated based on the amount of lubricant and open cavitation. The dynamic equation predicts the motion for each component, such as eccentricity of the piston and attitude angle of the bearing. For a more accurate prediction, these equations are calculated for each crank angle.

2. Testing method

In this work, the experimental strip-down method was conducted on a light duty vehicle diesel engine. The test was performed on a 1.99 L displacement engine with a bore of 84 mm and a stroke of 90 mm. The maximum engine power is 136.9 kW and the peak torque is 402.2 Nm. A five-stage engine strip down test was performed under motored engine conditions with controlled temperature. The coolant and oil temperature were held constant at 90 °C±1 using an external pump for cooling. The oil heater controller in the oil tank adjusted the power of the heater by PID control according to the set tem-

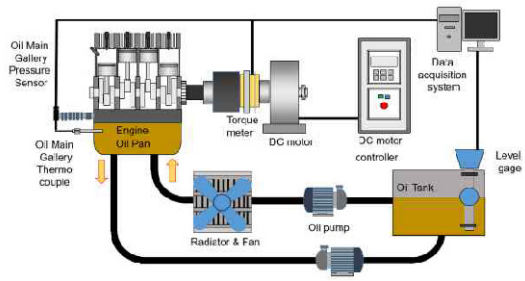

Fig. 1. Schematic diagram of the test engine system.

perature. In this process, the radiator and the fan were always activated. In addition, the main oil gallery pressure was controlled to the same motored complete engine conditions at each engine speed after the oil pump was removed. The amount of oil entering the main oil gallery was held constant through an external oil pump during the torque measurement steps. Changes in the oil supply affect engine friction, so the oil supply was verified using the level gage in the oil fan and external oil tank. The friction torque was measured under the controlled oil and coolant temperature at engine speeds from 1000 rpm to 4000 rpm (500 rpm step). The torque sensor signal was measured by a non-contact torque transducer with a maximum of 1000Nm and an accuracy of 0.03 % (T12, HBM). The data were acquired using the T12 assistant software provided by HBM. The test engine was motored for 30 min at an engine speed 2000 rpm to attain stability before torque measurements. To accurately measure the torque, constant experimental conditions were maintained for at least 3 minutes. Additional experimental data were acquired using a data acquisition hardware device (NI USB-6343, NI) with the NI LabVIEW software. Fig. 1 shows a schematic diagram of the test engine system.

To estimate each engine component, the test engine was disassembled in five steps.

Step 1 – The complete test engine is set up and measured for the friction measurement of the entire engine.

Step 2 – The auxiliaries are each disassembled sequentially from the test engine, such as water pump, front end accessory drive (FEAD) belt, common rail pump, vacuum pump, balance shaft module, and oil pump.

Step 3 – The cylinder head is disassembled from the complete test engine and replaced by a dummy plate. Only crank train components were retained in this step. The role of the dummy plate is to imitate the cylinder head, so it is machined to have the function as the cylinder liners with the same weight [7]. The dummy plate blocked oil and coolant passages, and the combustion chambers were exposed to the atmospheric pressure. In addition, tightening the cylinder head bolts affected engine friction due to the distortion of the cylinder bore [6, 28].

Step 4 – The piston assembly and connecting rods are disassembled from step 3 and replaced by dummy ring weights fixed to the crank pin. The dummy ring weights compensated the rotating mass of the piston assembly and connecting rods resulting from the imbalance caused by the removal of the piston assembly and connecting rods [28]. The dummy ring weights are equal to the rotating mass (the weights of the big end bearing and the part of the connecting rod at the crank pin) plus one-half of the reciprocating mass (the weights of the piston, piston ring, piston pin, and the part of the connecting rod at the piston pin) [29]. The friction in step 4 includes the friction of the main bearing and the friction between crankshaft and oil seals.

Step 5 – The dummy plate was disassembled, and the valve train and cylinder head were assembled from step 4. This step is for friction measurement of the valve train.

The friction of each component is determined as follow:

- Auxiliary components: The friction loss at step 2, difference before and after each part removal.
- Crankshaft group: The friction loss at step 4.
- Piston assembly & connecting rod (PIS & CON) group: 'The friction loss at step 3' – 'the friction loss at step 4'.
- Valve train group: 'The friction loss at step 5' – 'the friction loss at step 4'.

The friction loss of each component was determined from each torque measurement. The friction mean effective pressure (FMEP) was calculated using Eq. (1)

$$P_f = \frac{4\pi T}{v_d} \tag{1}$$

where P_f is the FMEP measured at torque T, for an engine displacement volume v_d [30].

3. Theoretical model

3.1 Friction modeling for piston skirt

In this research, the geometry shown in Figs. 2 and 3 is used as a reference, since some terms are different in each of the coordinate systems of previous studies. In this coordinate system, the center of the combustion cylinder top is set to the origin of the coordinates. The dynamic equation is based on force and moment equilibrium. In this piston geometry, the force equilibrium equation and the moment equation can be obtained based on the force applied to the piston, inertia, and friction. The reciprocating motion of the piston can be written as follows:

$$\begin{bmatrix} m_{pis}\left(1-\frac{a}{L}\right)+m_{pin}\left(1-\frac{b}{L}\right) & m_{pis}\left(\frac{a}{L}\right)+m_{pin}\left(\frac{b}{L}\right) \\ m_{pis}\left(1-\frac{a}{L}\right)(b-a)+\frac{I_{pis}}{L} & m_{pis}\left(\frac{a}{L}\right)(b-a)-\frac{I_{pis}}{L} \end{bmatrix} \begin{bmatrix} \ddot{e}_t \\ \ddot{e}_b \end{bmatrix} = \begin{bmatrix} F_{(1,x)}-F_{(1,y)}\tan\phi-F_A \\ M_n+M_f+M_s \end{bmatrix} \tag{2}$$

$$F_A = \left[F_{gas}+(m_{pis}+m_{pin})(g-\ddot{Y})\right]\tan\Phi \tag{3}$$

$$M_s = F_{gas}C_p - m_{pis}(g-\ddot{Y})C_c \tag{4}$$

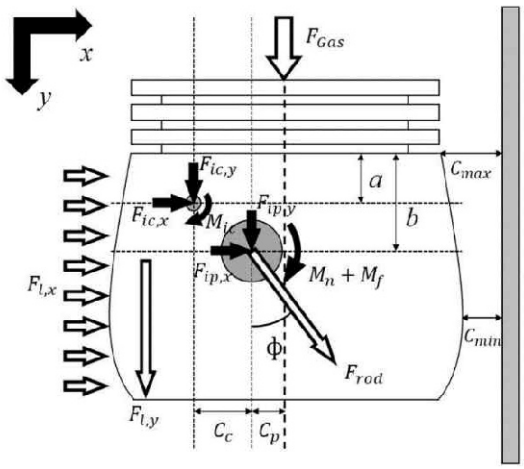

Fig. 2. Forces and moments acting on piston.

The variables e_t and e_b represent the eccentricities of the piston measured at the top and bottom of the skirt. $F_{(1,x)}$ is the normal force due to asperity contact pressure and hydrodynamic pressure from the oil film between the piston and cylinder, $F_{(1,y)}$ is the friction force due to asperity contact pressure and hydrodynamic pressure from the oil film, and these forces were defined by Zhu et al. [11]. The dynamic equation is used to predict piston movement, represented by e_t and e_b, but the piston friction due to contact and hydrodynamic pressure are unknown. To obtain the piston friction, the equation modeling oil film action between the piston skirt and the cylinder liner must be solved.

The equations used for simulation are based on the Reynolds equation to calculate the oil pressure at the piston skirt. To reflect the actual physical phenomena, it is necessary to add the roughness and waviness values of the materials to the Reynolds equation. In this study, we applied the approximation suggested by Patir and Cheng [14, 15], where an average Reynolds equation, including values of roughness and flow factors, is utilized.

The equation of the oil film lubrication between the piston skirt and cylinder liner can be written as follows:

$$\frac{\partial}{\partial\theta}\left[\Phi_x h^3\frac{\partial p}{\partial\theta}\right]+R^2\frac{\partial}{\partial\lambda}\left[\Phi_y h^3\frac{\partial p}{\partial\lambda}\right] = -6\mu UR^2\left(\frac{\partial h}{\partial\lambda}+\sigma\frac{\partial\Phi_s}{\partial\lambda}\right)+12\mu R^2\frac{\partial h}{\partial t} \tag{5}$$

where θ is the piston circumferential coordinate, λ is the piston axial coordinate, h is the oil film thickness between the piston skirt and the cylinder liner, and p is the oil pressure applied the piston skirt. Φ_x and Φ_y are the pressure flow factors, Φ_s is the shear flow factor, and σ is the roughness. To calculate the oil pressure from this equation, the functions for the oil film thickness and the roughness factors should be defined. The roughness factors are described in Ref. [15], and the surface pattern parameters are assumed to be isotropic roughness structure in Ref. [14]. The oil film thickness can be determined from the skirt liner geometry in Fig. 3 and is written as follows:

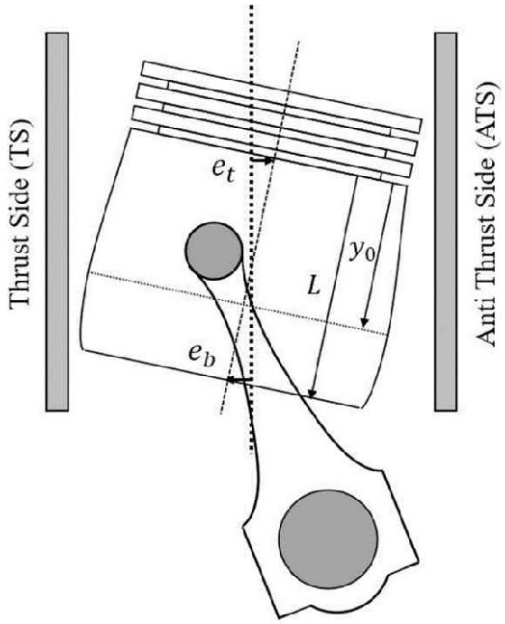

Fig. 3. Geometry system for piston and cylinder liner.

$$h(\theta,\lambda) = C(\lambda)+e_t\cos\theta+\frac{\lambda}{L}(e_b-e_t)\cos\theta \tag{6}$$

$$C(\lambda) = C_{\min}+\frac{C_{\max}-C_{\min}}{y_0^{\,2}}(\lambda-y_0)^2 \tag{7}$$

where $C_{\max}$ is the maximum radial clearance between the skirt and the liner, $C_{\min}$ is the minimum radial clearance, and y_0 is the vertical distance from the top of the skirt to the peak point where the minimum clearance is located. To determine the local oil film pressure, Eq. (5) was solved at the local position of the piston skirt using Eqs. (6) and (7). Additionally, the initial values for the piston movement and the boundary conditions for the piston skirt are needed to determine the piston motion and friction. The initial values are given as follows:

$$e_t(t_0)=0,\ e_b(t_0)=0,\ \frac{d^n}{dt^n}e_t(t_0)=0,\ \frac{d^n}{dt^n}e_t(t_0)=0 \tag{8}$$

where $t_0=0,\ n=1$ (velocity), and $n=2$ (acceleration). The boundary conditions are as follows:

$$p(\theta,0)=p(\theta,L)=p(\theta_{TS},\lambda)=p(\theta_{ATS},\lambda)=0 \tag{9}$$

$$\frac{\partial}{\partial\theta}p(0,\lambda)=\frac{\partial}{\partial\theta}p(\pi,\lambda)=0 \tag{10}$$

where θ_{TS} and θ_{ATS} are the end sides for each position. From these initial values and boundary conditions, the initial oil film thickness can be determined, so friction can be obtained

from the lubricant equation. Using these friction values, the subsequent motion of the piston can be calculated from the dynamic equation. Through the iterative calculation for one cycle (two strokes), the FMEP for the piston skirt can be calculated. The friction force is determined by viscous friction due to lubricant hydrodynamic pressure and asperity contact friction by direct contact between surfaces and can be written as follows:

$$F_f = \iint \tau dA + c_f \iint p_c dA_c \tag{11}$$

$$\tau = \frac{h}{2}\frac{\partial p}{\partial x} - \mu\frac{U}{h} \tag{12}$$

$$p_c = \begin{cases} 0, & \frac{h}{\sigma} > 4 \\ K'E'F_{2.5}\left(\frac{h}{\sigma}\right), & \frac{h}{\sigma} < 4 \end{cases} \tag{13}$$

$$K' = \frac{16\sqrt{2}}{15}\pi(N\beta'\sigma)^2\sqrt{\frac{\sigma}{\beta'}} \tag{14}$$

$$E' = \frac{2}{\left(\frac{1-\nu_1^2}{E_1} + \frac{1-\nu_2^2}{E_2}\right)} \tag{15}$$

where p_c is the asperity contact pressure, N is the number of asperities per unit contact area, β' is the asperity radius of curvature, σ is the variance of the composite surface roughness, ν_1 and ν_2 are Poisson's ratio, and these parameters were described by Greenwood et al. [31]. The function of $F_{2.5}$ presents the probability distribution of asperity height. Although the height of a particular asperity is random, the distribution of the asperity heights is rather close to Gaussian distribution. The model for average asperity contact pressure was established in Ref. [31]. According to Greenwood-Tripp's asperity contact model in Ref. [31], taking into account the distribution of asperity heights, the model surface could be used to predict some properties of actual surfaces. The expected total force and a total area of contact between the surfaces were affected by the statistical distribution of the sum of pairs of asperity heights. In Ref. [31], the normalized gap H_σ between contact surfaces was used to calculate the standardized height distribution and can be written as follow:

$$H_\sigma = \frac{h}{\sigma} \tag{16}$$

$$\sigma = \sqrt{\sigma_1 + \sigma_2} \tag{17}$$

where σ_1 and σ_2 are the standard deviations of the asperity height distributions on both surfaces. The gap h is a distance between the reference planes of the surfaces. σ_1 is determined by the asperity height from the reference plane of surface 1, and σ_2 is equal to σ_1. Hu et al. [32] used a power law approximation for $F_{2.5}(H_\sigma)$ in the form of Eq. (13). The range of validated normalized gap was determined at the first point of contact between two surfaces. The highest asperity on an actual surface is finite and the expected greatest height for Gaussian distribution is 4.04 σ in the Ref. [31]. The power loss can be written as follow:

$$P_f = \iint \mu\frac{U^2}{h}dA + \iint \frac{h^3}{12\mu}(\nabla p)^2 dA \tag{18}$$

3.2 Friction modeling for piston ring

The piston ring pack is used to seal the combustion gas in the combustion chamber, but blow-by gas leaks into the gap between the piston ring and the piston groove and moves into the orifice area, as shown in Fig. 4. Modeling of the blow-by gas was conducted in previous studies [32-35]. To analyze the blow-by gas flow, the forces by inertia and pressure difference between the top and the bottom of the ring, viscosity friction for lubricant between the cylinder liner and the ring, and squeeze effect for lubricant between the piston groove and the ring were used. The position of the piston ring is determined from the force equilibrium for these forces. The force equilibrium equation is written as follows, and each term was described in Ref. [17]:

$$0 = F_{inertia} + F_{pressure} + F_{viscosity} + F_{squeeze} \tag{19}$$

$$F_{inertia} = -m_{ring,nth}\frac{d^2y}{dt^2} \tag{20}$$

$$F_{pressure} = A_r\left(p_b - p_t\right) \tag{21}$$

$$F_{viscosity} = \left(4.8\sqrt{\frac{\mu U_{pis}}{(p_{back}+p_{ten})h_{groove}}}\right)\pi D\left(p_{back}+p_{ten}\right)h_{groove} \tag{22}$$

$$F_{squeeze} = -(0.1)2\pi\mu R_i\frac{dh_{channel}}{dt}\left(\frac{w}{h_{channel}}\right)^3 \tag{23}$$

To solve this equilibrium equation, the initial conditions are given as follows:

$$\begin{cases} p_2(\theta_0) = p_{comb}(\theta_0) - \left[p_{comb}(\theta_0) - p_{atm}\right]/4 \\ p_3(\theta_0) = p_{comb}(\theta_0) - 2\left[p_{comb}(\theta_0) - p_{atm}\right]/4 \\ p_4(\theta_0) = p_{comb}(\theta_0) - 3\left[p_{comb}(\theta_0) - p_{atm}\right]/4 \\ p_5 = p_{atm} \text{ (all crank)} \end{cases} \tag{24}$$

$$\begin{cases} h_{channel,1\to2}(\theta_0) = h_{groove,1st} - h_{ring,1st} \\ h_{channel,2\to3}(\theta_0) = 0 \\ h_{channel,3\to4}(\theta_0) = h_{groove,2nd} - h_{ring,2nd} \\ h_{channel,4\to5}(\theta_0) = 0 \end{cases} \tag{25}$$

Using these conditions, the piston ring position for each crank angle is calculated based on the channel height. The internal pressure between the rings for each crank angle is also calculated. After calculating the results of these blow-by effects, and the lubricant analysis for each ring, it is possible to calculate the film thickness and the friction and power loss.

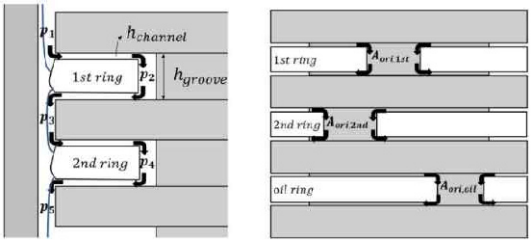

Fig. 4. Piston ring orifice and blow-by gas between ring and groove.

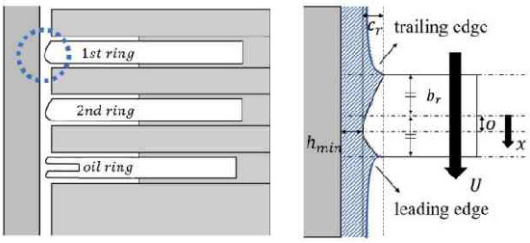

Fig. 5. Geometry for piston ring.

In this paper, the model of the piston ring is assumed to be axial symmetry and one-dimensional. The Reynolds equation can be written as:

$$\frac{\partial}{\partial x}\left(\frac{h^3}{12\mu}\frac{\partial p}{\partial x}\right)=\frac{1}{2}U\frac{\partial h}{\partial x}+\frac{\partial h}{\partial t} \tag{26}$$

As shown in Fig. 5, the piston ring pack consists of two compressed rings and one twin-rail oil ring. While the ring pack moves in the cylinder, the lubricant at the cylinder wall seeps into the gap between the piston ring and the wall. The boundary of the piston rings is related to a leading edge and a trailing edge, depending on the direction of piston motion. In this paper, it is assumed that the lubricant at the cylinder is sufficient. The surface of each ring is barrel-shaped because it is resistant to high-pressure combustion gas. The ring shape can be defined by a follow equation:

$$h(x,t)=h_m(t)+\frac{C_r}{(b/2+o)^2}(x-o)^2 \tag{27}$$

To solve the Reynolds equation, the boundary conditions of the piston ring should be considered. When the piston is moving, the wedge effect is mainly applied to the lubricant due to the relative speed between the ring and the cylinder, resulting in cavitation. When the piston is located at top dead center (TDC) or bottom dead center (BDC), the squeeze effect is applied to the lubricant, so cavitation does not occur. Reynolds cavitation boundary conditions, shown in Fig. 6, are most commonly used for cavitation analysis. This condition assumes that the enclosed cavitation occurred in the oil film, and then the oil film is formed again. However, an open cavitation boundary condition, shown in Fig. 6, was used for cavitation analysis in this paper. This condition was recently proposed

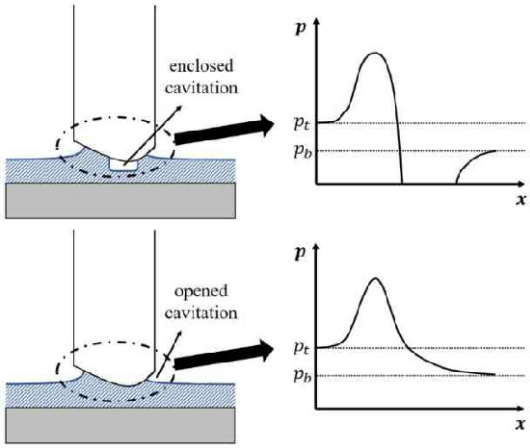

Fig. 6. The boundary condition for Reynolds and opened cavitation.

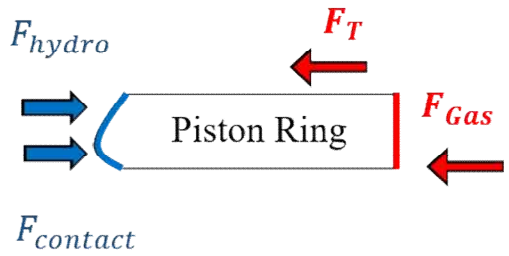

Fig. 7. Free body diagram of piston ring.

and assumes that the gas at the back of the piston ring is cavitation. The boundary conditions for open cavitation and no cavitation are as follows:

$$(\text{Cavitation}):\ P(x_{outlet})=P_{gas,outlet},\ x_{inlet}=\frac{b}{2} \tag{28}$$

$$(\text{No cavitation}):\ P(x_{outlet})=P_{gas,outlet},\ x_{outlet}=\frac{b}{2} \tag{29}$$

In addition, the quasi-steady state problem was applied to the friction modeling of the piston ring to the cavitation boundary location. Fig. 7 shows the forces acting on the piston ring. The tension of the ring in the radial direction $F_{tension}$, the force due to gas pressure on the inner face of the ring F_{gas}, the force due to hydrodynamic pressure of the lubricant film F_{hydro}, and the force caused by direct asperity contact between the ring surface and cylinder liner surface $F_{contact}$ were applied to piston ring. The force equilibrium condition can be expressed as:

$$W_{external}=F_t+F_{gas}=F_{hydro}+F_{contact} \tag{30}$$

The sum of F_{hydro} and $F_{contact}$ corresponds to the normal load on the friction surface between the piston ring and the cylinder liner. During the reciprocating motion of the piston, the lubrication condition at the piston ring is fully flooded or starved. The lubrication condition at only the 2nd rail of the oil ring is

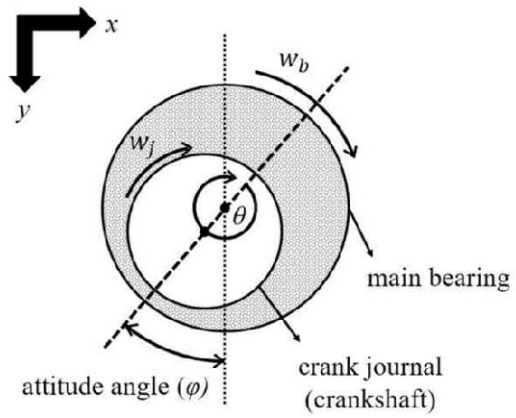

Fig. 8. Geometry for journal bearing.

fully flooded during down stroke, and the remaining rings are moved at starved lubrication condition during all stokes. The boundary conditions for fully flooded and starved lubrication are as follows:

$$\text{(Fully flooded)}: \; P\left(x_{inlet}\right)=P_{gas,inlet}, \; x_{inlet}=\frac{b}{2} \tag{31}$$

$$\text{(Starved)}: \; P\left(x_{inlet}\right)=P_{gas,inlet}, \; q_{inlet}=q_{available} \tag{32}$$

Using these boundary conditions, the minimum thickness and the effective lubricant width of each ring are calculated based on the crank angle. From these results, the friction force and the power loss for the piston ring were determined. The calculation procedure of the friction force and the power loss is the same as that described in the case of the piston skirt. The total friction force is the sum of viscous friction force caused by the lubricant viscosity and the contact friction force caused by direct asperity contact between piston ring surface and cylinder liner. The lubricant was assumed to be Newtonian fluid and the total friction force of the piston ring is determined from Eq. (11).

3.3 Friction modeling for journal bearing

Fig. 8 shows the journal bearing geometry and coordinate system. The Reynolds equation for the journal bearing in a polar-coordinate system is described by Booker [25], and can be written as follow:

$$\begin{aligned}&\frac{\partial}{\partial\theta}\left(h^3\frac{\partial p}{\partial\theta}\right)+R^2\frac{\partial}{\partial z}\left(h^3\frac{\partial p}{\partial z}\right)\\&=12\mu R^2c\left[\dot{\varepsilon}\cos\theta+\varepsilon\left(\dot{\varphi}-\bar{\omega}\right)\sin\theta\right]\end{aligned} \tag{33}$$

where $\dot{\phi}$ is the angular velocity of the attitude angle, $\bar{\omega}$ is the average angular velocity of the journal and bearing relative to the force acting on the journal, and ε is the eccentricity ratio. The thickness of the lubricant film is then:

$$h=c\left(1+\varepsilon\cos\theta\right) \tag{34}$$

The journal bearing is filled with lubricant, so its circumferential period is from 0 to 2π. However, in the real case, negative pressure does not occur, so the boundary conditions are written as follows:

$$\text{Short bearing}\left(\frac{L}{D}\le 0.5\right):$$

$$\theta_1=\tan^{-1}\frac{\dot{\varepsilon}}{\varepsilon\left(\bar{\omega}-\dot{\varphi}\right)}, \; \theta_2=\begin{cases}\theta_1+\pi, \; \varepsilon\left(\bar{\omega}-\dot{\varphi}\right)>0\\ \theta_1-\pi, \; \varepsilon\left(\bar{\omega}-\dot{\varphi}\right)<0\end{cases} \tag{35}$$

$$\text{Long bearing}\left(\frac{L}{D}>0.5\right):$$

$$\theta_1=\tan^{-1}\frac{\left(2+\varepsilon^2\right)\dot{\varepsilon}}{2\varepsilon\left(\bar{\omega}-\dot{\varphi}\right)}, \; \theta_2=\begin{cases}\theta_1+\pi, \; \varepsilon\left(\bar{\omega}-\dot{\varphi}\right)>0\\ \theta_1-\pi, \; \varepsilon\left(\bar{\omega}-\dot{\varphi}\right)<0\end{cases} \tag{36}$$

Using these boundary conditions, the Reynold equation is solved, and the pressure distribution is calculated. Due to the pressure distribution, the location of the journal center changes, and the mobility is a dimensionless ratio of velocity to force which is affected by the journal center location as:

$$\dot{\varepsilon}=\frac{F_{main}\left(c/R\right)^2}{\mu LD}M^{\varepsilon}, \; \dot{\varphi}=\frac{F_{main}\left(c/R\right)^2}{\mu LD\varepsilon}M^{\varphi}+\bar{\omega} \tag{37}$$

$$M^{\varepsilon}=M^{\xi}\cos\varphi+M^{\kappa}\sin\varphi, \; M^{\varphi}=M^{\kappa}\cos\varphi-M^{\xi}\sin\varphi \tag{38}$$

$$M^{\xi}=\frac{\left(1-\xi\right)^{5/2}}{\pi\left(L/D\right)^2}, \; M^{\kappa}=\frac{4\kappa\left(1-\xi\right)^{3/2}}{\pi^2\left(L/D\right)^2} \tag{39}$$

$$\xi=\varepsilon\cos\varphi, \; \kappa=\varepsilon\sin\varphi \tag{40}$$

The force applied to the center main bearing was calculated from the model in Ref. [36]. Integrating the calculated rate of the eccentricity ratio ($\dot{\varepsilon}$) and the attitude angle ($\dot{\varphi}$), the journal center location and the journal bearing centerline are obtained. The initial values for the eccentricity ratio and the attitude angle are 0.7 and 1.5 rad. Through a time-step, the pressure distribution for each crank angle can be calculated, and the friction force of the journal bearing can be obtained from Eq. (41)

$$F_{f,bearing}=\iint\tau dA=\frac{2\pi\mu URL}{c\sqrt{1-\varepsilon^2}} \tag{41}$$

For oil seal, the seal friction modeling in Ref. [37] was used in this study. The total friction torque was determined from the seal lip force, the contribution of the material to the seal friction force, and the shaft diameter.

4. Results and discussion

4.1 Simulation validation and friction characteristics of crank train components

Friction characteristics are influenced by the friction coefficient and the lubrication regime. These factors are determined through a friction theory, called the Stribeck curve, as shown in

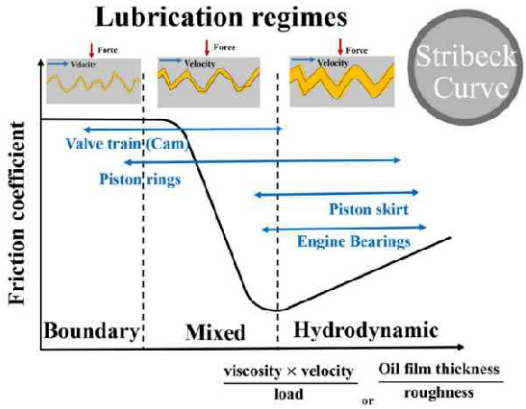

Fig. 9. Lubrication regimes of engine components.

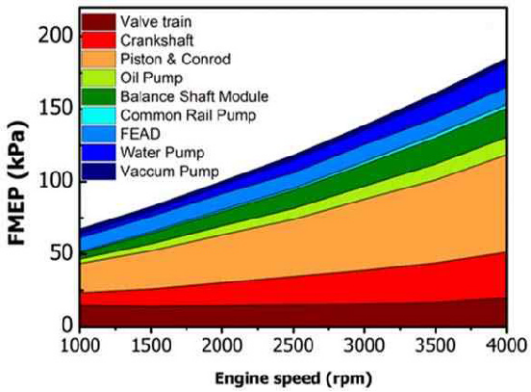

Fig. 10. Friction loss measured from strip down method under motored conditions.

Fig. 9 [38]. Bovington studied the change of lubrication characteristics by various variables related to the Stribeck curve [39]. Similarly, the Stribeck curve was used to analyze the friction characteristics of crank train components for various engine operating conditions.

The obtained distribution of measured friction loss for various components was analyzed using the strip-down method as shown in Fig. 10. As shown in Fig. 10, the friction loss of the crank and valve train account for at least 62 % to 65 % of the total. The components of the crank train include the top, second, and oil piston rings, the piston skirt, the small and big end bearings of the connecting rods, the crankshaft main bearing, and the crankshaft seals. The friction loss of the crank train contributes at least 42 % and possibly up to 53 % of the total. The strip-down method is considered at the opened cylinder condition, so the friction loss due to crankcase gas is not included in this friction loss of the crank train. However, the crankcase gas is an important factor affecting the friction of the crank train. Crankcase gas creates resistance to piston motion, up and down, as well as connecting rods and crankshaft movement [6]. Crank train friction under fired engine conditions is higher than that under motored engine conditions due to the effects of high combustion gas pressure and temperature during the power stroke [39, 40]. The estimation of crank train

Table 1. Engine specifications and input parameters.

Definition	Values
Bore	84 mm
Stroke	90 mm
Connecting rod length	145 mm
Composite roughness (skirt)	0.6 μm
Skirt clearance	75 μm
Composite roughness (ring)	0.37 μm
Piston first ring height	2.61 mm
Piston second ring height	2.06 mm
Piston oil ring height	3.02 mm
Main bearing diameter	60 mm
Main bearing clearance	44 μm
Oil viscosity (5W-30 / temp: 90 °C)	0.01022 Pa.s
Friction coefficient for dry contact	0.15

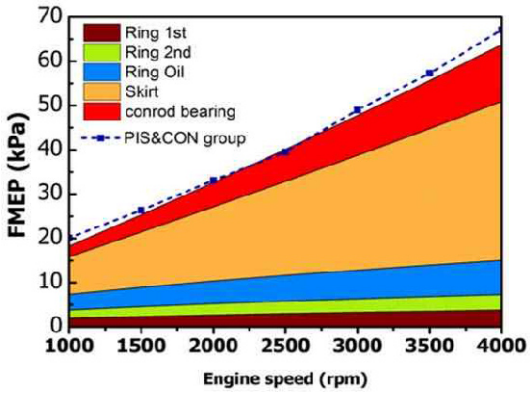

Fig. 11. Comparison between measured and calculated FMEP of PIS&CON group.

friction is important because its contribution differs under motored and fired engine conditions. The friction loss of all components except the valve train increased with engine speed.

The numerical models for crank train friction are validated against experimental data in terms of each component FMEP. The engine specifications and input parameters are presented in Table 1. Since it is not possible to divide detailed losses such as the respective piston ring losses using any known measurement technique [6], the FMEP for each group of Sec. 2 is compared to the sum of each component FMEP calculated using a different model. The friction of PIS & CON group includes the friction losses between the top, second, oil piston ring, piston skirt, connecting rods, and the small and big end bearings. In the numerical analysis of the PIS & CON group, the friction loss of the small end bearings was ignored as insignificant when compared to the big end and the main bearings [41]. A comparison between the measured and calculated results of PIS & CON is described in Fig. 11. The piston skirt FMEP occupies a large portion of the total FMEP since the area of contact between the piston skirt and the cylinder liner is

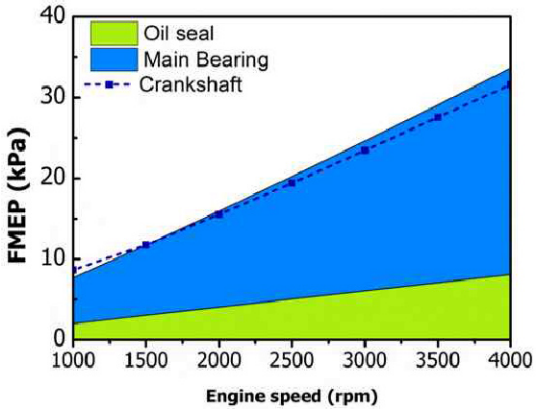

Fig. 12. Comparison between measured and calculated FMEP of crankshaft group.

larger than that of other components. In the case of piston rings, the FMEP of the oil ring is the highest due to high ring tension. The asperity contact friction of the piston in the boundary lubrication regime occurred near TDC [42]; however, the overall trend of FMEP is included in the hydrodynamic lubrication regime. The measured and calculated data of PIS & CON have an average error of 3 % based on the measured data.

A comparison of the crankshaft group is shown in Fig. 12. The FMEP of the main bearing accounts for the overwhelming proportion of the crankshaft group. There is an average error of 5 % based on the measured data in Fig. 12. The linear correlation between FMEP and engine speed was investigated. All FMEP of components, such as PIS & CON, and crankshaft group, increased with engine speed because the component friction behaves predominantly in the hydrodynamic lubrication regime [43]. The difference between the measured FMEP and the calculated FMEP of the crankshaft increased with engine speed because the calculated results did not take into account the oil film inertia effect [44].

Fig. 13 shows the calculated results for the friction characteristics of the piston's first compression ring. Oil film thickness is an important factor influencing friction characteristics [45]. The oil film thickness measurement increases the understanding of the phenomena leading to friction between the contact surfaces of engine components. Through oil film thickness analysis, the characteristics of friction force and power loss can be grasped, and it is possible to predict which lubrication regime corresponds to this. The cylinder pressure increased with increasing load, which reduced the thickness of the oil film. The lubrication regime in the motored case is hydrodynamic at almost every stroke; however, the boundary lubrication regime is slightly distributed near TDC and BDC. When the piston sliding velocity approaches zero and its direction changes, squeeze film effects occurred to retain some of the oil film thickness [46]. The minimum oil film thickness was nearly zero at TDC following the compression stroke due to the overwhelming squeezing film effect. The consequence of this phenomenon is the transition from hydrodynamic to boundary lubrication. In addition, the

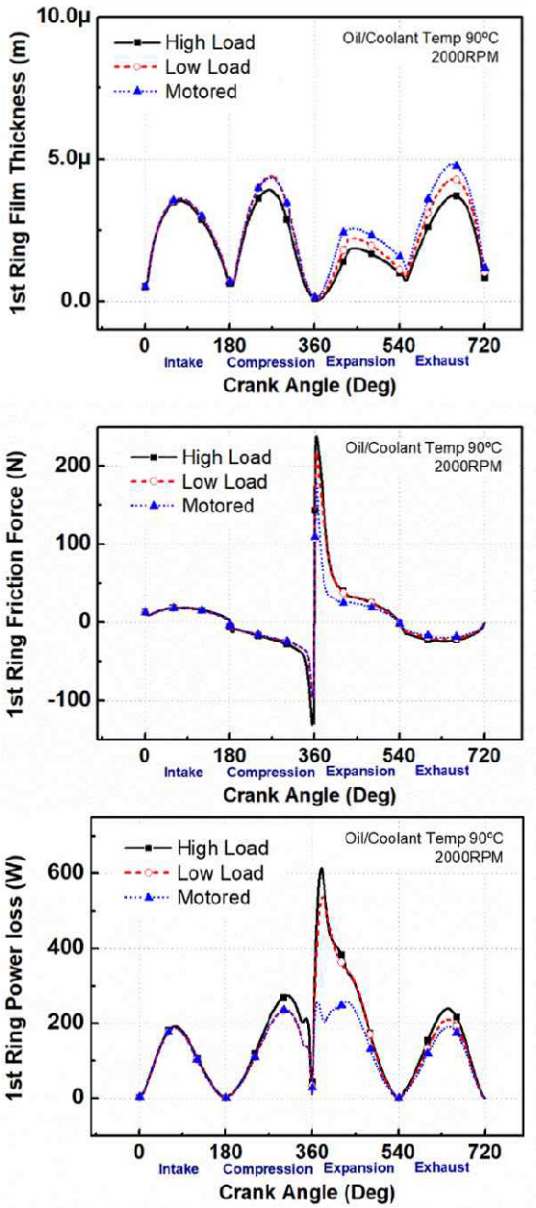

Fig. 13. Minimum oil film thickness, friction force and power loss of first ring under various load conditions.

minimum oil film thickness decreases with engine load. The friction force by direct asperity contact increased suddenly due to cylinder pressure at TDC. The total friction force similarly increased with engine load. The power loss of the first compression ring had a peak near the middle of the stroke, except during the expansion stroke. This is because the piston sliding velocity has a large influence on the friction power loss calculation. Although the piston sliding velocity is very low, there was a peak power loss near TDC due to a very large friction force in the expansion stroke. Analogously, the first compression ring power loss increases with engine load at the compression stroke.

In the case of the piston's second ring, the calculated result

for friction characteristics is similar to that of a first compression ring, as shown in Fig. 14. The behavior of the second compression ring is less affected by engine load than that of the first compression ring. This is because the inter-ring gas pressure is much lower than the cylinder pressure, as shown in Fig. 15. The engine combustion experiment was conducted using the single-cylinder engine manufactured to the same engine specification. The cylinder pressure was measured through experiments under motored, low load, and high load conditions. And these pressure data were used to calculate the inter-ring pressure. The inter-ring pressure was calculated through the mathematical model based on Ref. [18]. There was a difference in the impact of the engine load on power loss and

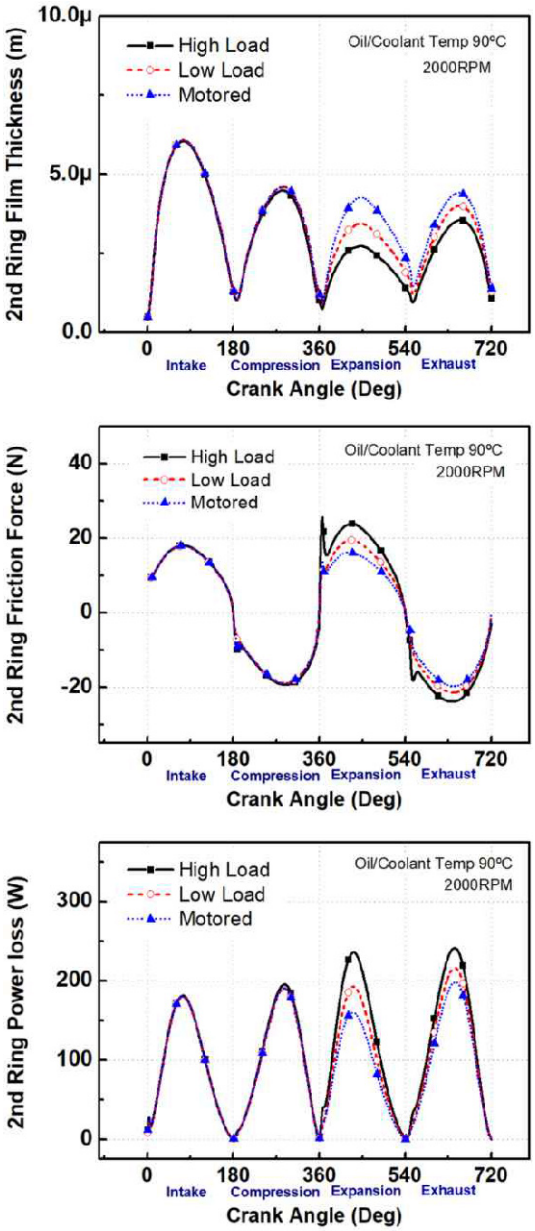

Fig. 14. Minimum oil film thickness, friction force and power loss of second compression ring under various load conditions.

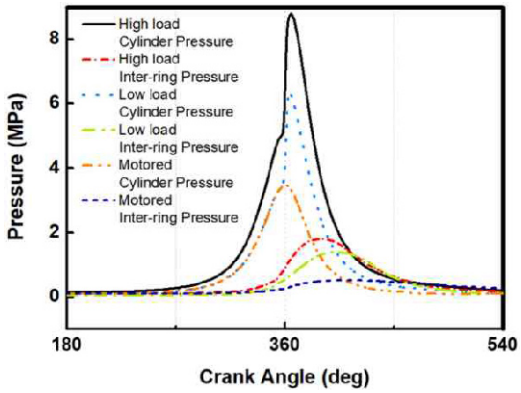

Fig. 15. Input cylinder pressure and inter-ring Pressure between first and second compression ring.

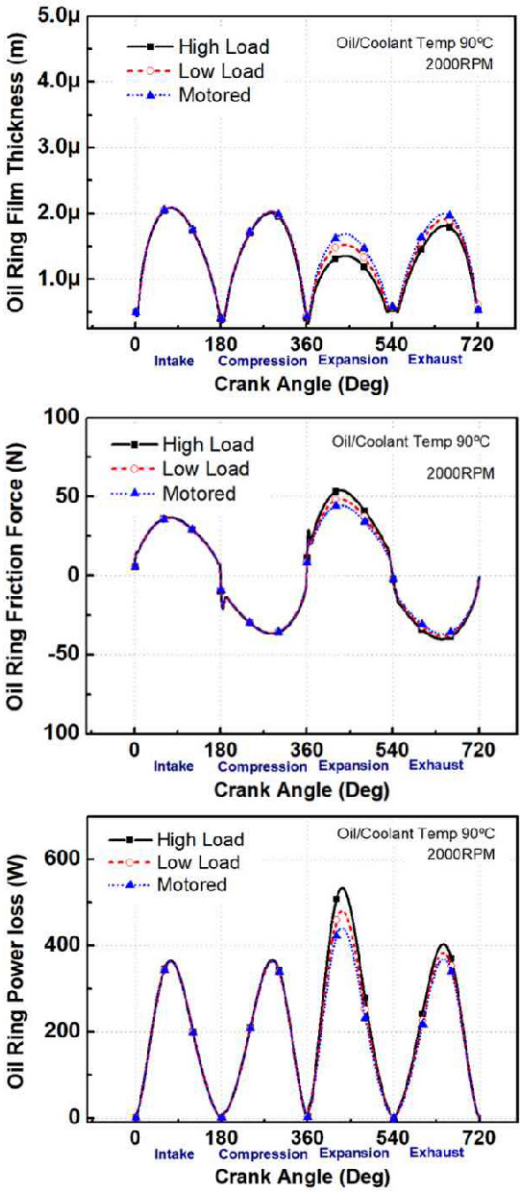

Fig. 16. Minimum oil film thickness, friction force and power loss of oil top ring under various load conditions.

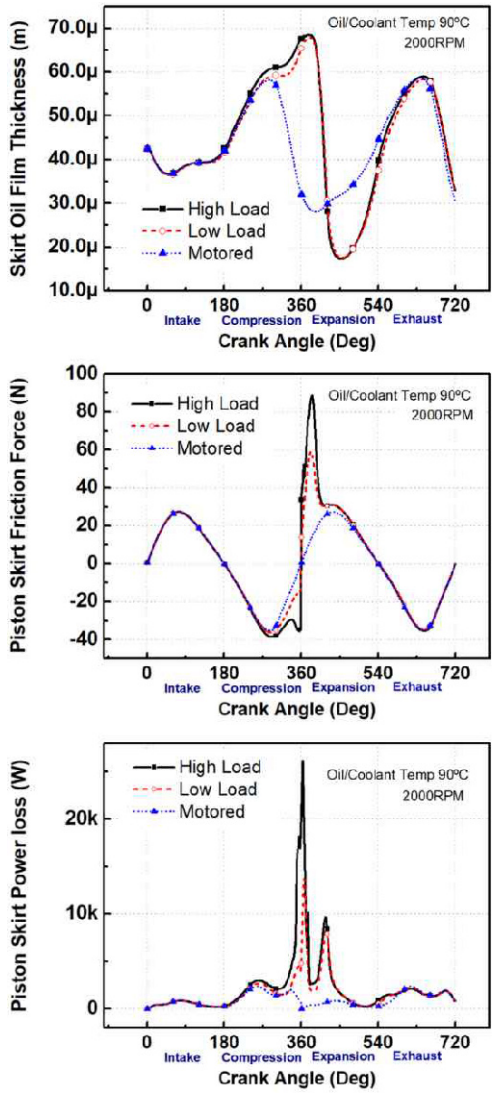

Fig. 17. Minimum oil film thickness, friction force and power loss of piston skirt under various load conditions.

frictional force.

The oil ring was handled as a separate single ring in the study. The friction of the piston oil top ring was least affected by the variation of engine load, as shown in Fig 15. The oil ring also exhibits a similar tendency to the second compression ring. The higher ring tension of the oil ring resulted in a lower minimum oil film thickness and higher asperity contact friction. Subsequently, the contribution of the boundary lubrication regime increased in the case of the oil ring. Therefore, the power loss of the oil ring is the highest among the piston rings.

In Fig. 17, the piston skirt friction characteristics differed with the piston ring. The amount of variation in the minimum oil film thickness between the piston skirt and the cylinder liner increased with the engine load. When cylinder pressure started to increase due to combustion, the minimum oil film thickness increased and then decreased after TDC. The piston skirts later motion by suddenly increased cylinder pressure created a

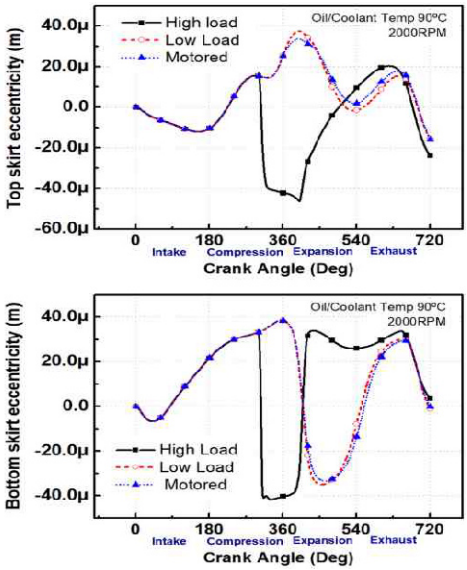

Fig. 18. Piston skirt eccentricity under various load conditions.

squeeze film effect and subsequently the minimum oil film thickness was reduced due to the squeeze film effect neglected by the high cylinder pressure. At the same time, the skirt friction increased due to reduced oil film thickness. In the case of power loss, the peak point occurs near the middle of the intake and exhaust stroke, as this is when maximum piston slide velocity occurs. The highest peak point occurs near TDC between the compression and expansion strokes. This is because the asperity contact friction increased due to the increased tilting motion of the piston skirt. The piston skirt eccentricity increased when cylinder pressure increased, as shown in Fig. 18.

The calculated results for the main bearing friction characteristics are presented in Fig. 19. Since the main bearing is loaded by connecting rods moving because of combustion, the eccentricity of the main bearing is changed for each crank angle. The minimum film thickness of the main bearing varied depending on the eccentricity of the main bearing. In Fig. 20, the load of the center bearing in an in-line four-cylinder engine was increased by the force transmitted by the connecting rod. When the engine load increased, the force transmitted to the main bearing by the connecting rod increases, affecting the eccentricity and the oil thickness. The friction force and power loss of the main bearing started to increase near TDC where cylinder pressure increased significantly.

4.2 Effect on temperature of engine oil and coolant

The crankshaft friction measurements were carried out at coolant, oil main gallery, and oil pan temperatures of 30 °C±2, 50 °C±2, 70 °C±2, and 90 °C ±2, respectively, under motored engine conditions, as shown in Fig. 21. The crankshaft friction increased with oil temperature reduction because the oil vis-

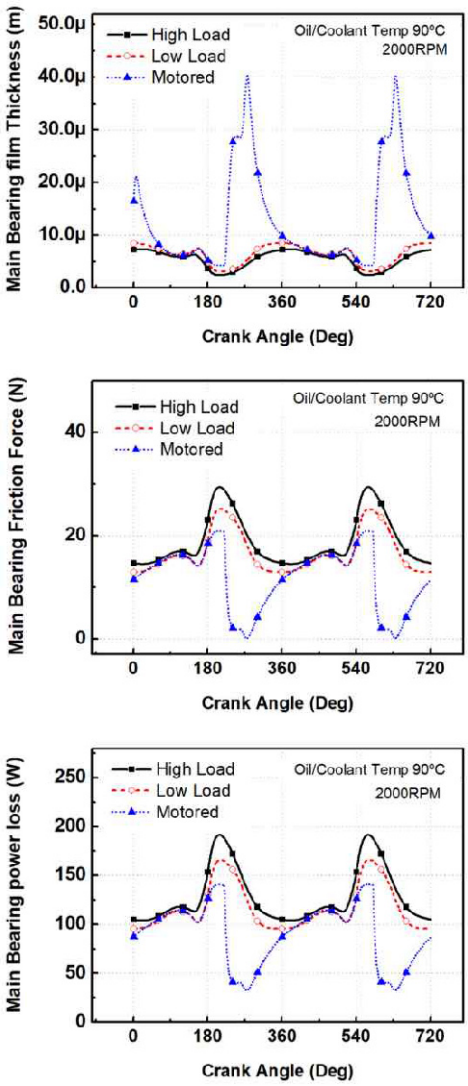

Fig. 19. Minimum oil film thickness, friction force and power loss of oil top ring under various load conditions.

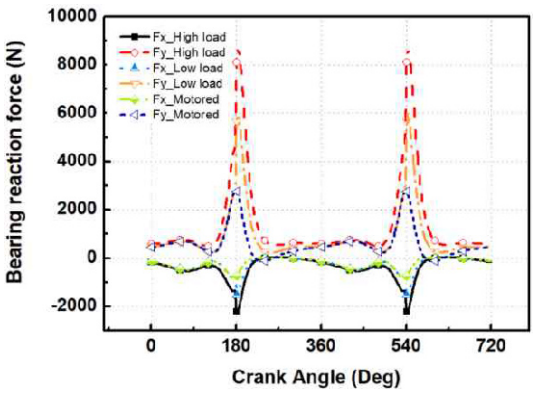

Fig. 20. Calculated forces on center main bearing.

cosity increased. This phenomenon is similar to the case of engine warm-up [47]. The lubrication of crankshaft friction at all temperatures is mostly included in the hydrodynamic lubrication regime due to the sufficient oil supply. Having enough oil supply for the main bearing is possible because oil holes in the main bearing journal are connected directly from the cylinder block oil to the main gallery. The sufficient oil supply enabled appropriate conditions for the hydrodynamic lubrication regime. In hydrodynamic lubrication, friction coefficients increase with oil viscosity according to the Stribeck curve. The engine oil temperature was measured between 80 °C and 100 °C under actual operating conditions [48]. To reduce crankshaft friction loss, it is necessary to reduce the friction losses of the engine warm-up. The FMEP increment between an oil temperature of 30 °C and 50 °C is higher than other temperature sections. This is because the oil viscosity increment at 30 °C is higher than that of other temperatures [49].

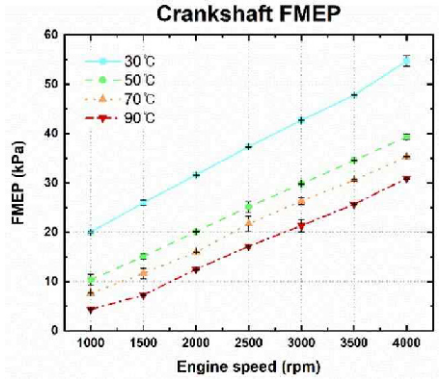

Fig. 21. Measured FMEP of crankshaft at various oil temperature.

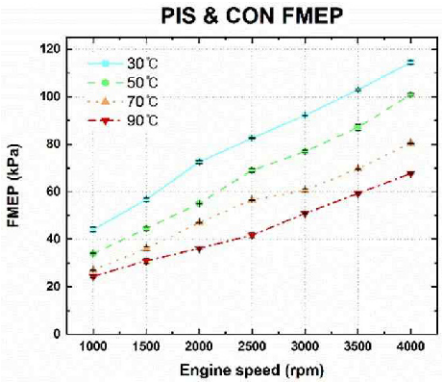

Fig. 22. Measured FMEP of PIS & CON at various oil temperature.

The same tendency was also observed in the PIS & CON FMEP measurement results and can be confirmed in Fig. 22. However, in the case of PIS & CON FMEP, the FMEP increment is relatively constant compared to the case of crankshaft FMEP. It was found that the contribution to the hydrodynamic regime in the PIS & CON FMEP is lower than in the case of crankshaft FMEP. This is because the friction of the piston ring is partially included in the boundary lubrication regime. In the boundary lubrication regime, the viscosity change does not influence the friction coefficient.

5. Conclusions

The following conclusions can be drawn from current work:

(1) Measured data from the strip-down method indicated the contribution of each engine component to the total friction under motored conditions. The crank train accounts for about 50 % of total engine friction loss. The FMEP of each engine component was almost in the hydrodynamic lubrication regime. The FMEP of all components, except the valve train, increased with engine rpm. The FMEP of the skirt and main bearing is estimated to be the largest proportion.

(2) Using a numerical model of the detailed components, the FMEP of each engine component group was compared to the sum of each detailed component FMEP and the correlation between measurement and calculation was investigated.

(3) After compression stroke, the minimum film thickness of piston rings decreased with engine load due to the force by the combustion gas pressure. The friction force and power loss of piston rings increased with engine load because the reduced oil film thickness resulted in low load carrying capacity and increased asperity contact friction. In the case of the oil ring, the effect of engine load variation was insignificant.

(4) The rate of change for eccentricity of the piston skirt and the crankshaft main journal increased during expansion stroke due to the force by the combustion gas pressure. The minimum film thickness of the piston skirt and the crankshaft main bearing decreased with engine load due to the variation of eccentricity. The friction force and power loss of the piston skirt and the crankshaft main bearing increased with engine load because the reduced oil film thickness resulted in low load carrying capacity and increased asperity contact friction.

(5) The effects of the engine oil and coolant temperature on the FMEP were analyzed through the measured FMEP of each engine component group. When oil temperature was low, the oil viscosity and the load carrying capacity of oil increased. Lower oil temperatures than the actual engine operating conditions increased the oil viscosity and engine component friction loss.

Acknowledgments

This work was supported by Basic Science Research Program through the National Research Foundation of Korea (NRF) (NRF-2018R1D1A1B07050092) and “Human Resources Program in Energy Technology” of the Korea Institute of Energy Technology Evaluation and Planning (KETEP), granted financial resource from the Ministry of Trade, Industry & Energy, Republic of Korea (No. 20184010201710).

Nomenclature

ATS : Anti-thrust side
BMEP : Brake mean effective pressure
FMEP : Friction mean effective pressure
HCCI : Homogeneous charge compression-ignition
IMEP : Indicated mean effective pressure
TS : Thrust side
a : Vertical distance between top of piston skirt and piston center of mass
A_r : Area of the piston ring from a top view
b : Vertical distance between top of piston skirt and piston pin center
b_r : Half of the piston ring thickness
c_b : Radial clearance between the journal and bearing
c_f : Coefficient of friction
c_r : Maximum distance of ring surface
C_c : Horizonal distance between the piston center of mass and the piston pin center
C_p : Horizonal distance between the piston center line and the piston pin center
D : Inner diameter of the piston ring
e_b : Eccentricity of piston at the skirt bottom
e_t : Eccentricity of piston at the skirt top
F_{gas} : Force obtained by pressure in the combustion chamber
F_{ic} : Inertia force at the piston center of mass
F_{ip} : Inertia force at the piston pin center
F_l : Friction force obtained by lubricant
F_{main} : Force applied to the center main bearing
F_{rod} : Force obtained by the connecting rod
$h_{channel}$: Height between the ring and groove
h_{groove} : Height of the groove
h_m : Minimum oil film thickness of the piston ring
I_{pis} : Rotational inertia of piston center of mass
L : Length from the skirt top to the bottom
m_{pis} : Mass of piston
m_{pin} : Mass of piston pin
$m_{ring,nth}$: Mass of piston nth ring
o : Piston ring offset
p : Hydrodynamic oil film pressure
p_{atm} : Atmosphere pressure
p_b : Pressure at the bottom of the piston ring
p_{back} : Pressure of the piston back face
p_c : Asperity contact pressure
p_t : Pressure at the top of the piston ring
p_{ten} : Pressure of the piston tension
U : Reciprocating velocity of the piston
φ : Angle between the vertical line of piston pin and the center line of the connecting rod
μ : Dynamic viscosity for lubricant

References

[1] K. Holmberg, P. Andersson, N.-O. Nylund, K. Mäkelä and A. Erdemir, Global energy consumption due to friction in trucks and buses, *Tribology International,* 78 (2014) 94-114.

[2] M. Hoshi, Reducing friction losses in automobile engines, *Tribology International,* 17 (1984) 185-189.

[3] Y. Zhou, H. Zhu, W. Tang, C. Ma and W. Zhang, Development of the theoretical model for the optimal design of surface texturing on cylinder liner, *Tribology International,* 52 (2012) 1-6.

[4] A. Usman and C. W. Park, Optimizing the tribological performance of textured piston ring–liner contact for reduced frictional losses in SI engine: Warm operating conditions, *Tribology International,* 99 (2016) 224-236.
[5] D. E. Richardson, Review of power cylinder friction for diesel engines, *Journal of Engineering for Gas Turbines and Power,* 122 (2000) 506-519.
[6] P. Carden et al., Calculation of crank train friction in a heavy duty truck engine and comparison with measured data, *Proceedings of the Institution of Mechanical Engineers, Part J: Journal of Engineering Tribology,* 227 (2012) 168-184.
[7] A. Krishnan, Simulation of an engine friction strip test, *Master's Thesis*, Chalners Univ. of Technology (2014).
[8] T. Sato, H. Kurita, A. Ito and H. Iwasaki, Friction measurement of Al-17%Si monolithic cylinder with using newly developed floating liner device, *SAE International Journal of Engines,* 8 (2014) 135-142.
[9] P. Carden, D. Bell, M. Priest and D. Barrell, Piston assembly friction losses: Comparison of measured and predicted data, *SAE International* (2006).
[10] T. Deuß, H. Ehnis, R. Rose and R. Künzel, Friction power measurements of a fired diesel engine–influence of piston skirt coatings, *MTZ Worldwide eMagazine,* 72 (2011) 18-23.
[11] D. Zhu, H. S. Cheng, T. Arai and K. Hamai, A numerical analysis for piston skirts in mixed lubrication—Part I: Basic modeling, *Journal of Tribology,* 114 (1992) 553-562.
[12] G. A. Livanos and N. P. Kyrtatos, Friction model of a marine diesel engine piston assembly, *Tribology International,* 40 (2007) 1441-1453.
[13] X. Meng and Y. Xie, A new numerical analysis for piston skirt–liner system lubrication considering the effects of connecting rod inertia, *Tribology International,* 47 (2012) 235-243.
[14] N. Patir and H. S. Cheng, An average flow model for determining effects of three-dimensional roughness on partial hydrodynamic lubrication, *Journal of Lubrication Technology,* 100 (1978) 12-17.
[15] N. Patir and H. S. Cheng, Application of average flow model to lubrication between rough sliding surfaces, *Journal of Lubrication Technology,* 101 (1979) 220-229.
[16] T.-W. Kuo, M. C. Sellnau, M. A. Theobald and J. D. Jones, Calculation of flow in the piston-cylinder-ring crevices of a homogeneous-charge engine and comparison with experiment, *SAE International* (1989).
[17] J. E. Yun, Variation of inter-ring gas pressure in internal combustion engine, *Transaction of the Korean Society of Automotive Engineers,* 3 (1995) 238-249.
[18] W. Chong, S. Howell-Smith, M. Teodorescu and N. Vaughan, The influence of inter-ring pressures on piston-ring/liner tribological conjunction, *Proceedings of the Institution of Mechanical Engineers, Part J: Journal of Engineering Tribology,* 227 (2013) 154-167.
[19] P. Lyubarskyy and D. Bartel, 2D CFD-model of the piston assembly in a diesel engine for the analysis of piston ring dynamics, mass transport and friction, *Tribology International,* 104 (2016) 352-368.
[20] Y.-R. Jeng, Theoretical analysis of piston-ring lubrication Part I—Fully flooded lubrication, *Tribology Transactions,* 35 (1992) 696-706.
[21] Y.-R. Jeng, Theoretical analysis of piston-ring lubrication Part II—Starved lubrication and its application to a complete ring pack, *Tribology Transactions,* 35 (1992) 707-714.
[22] D.-C. Han and J.-S. Lee, Analysis of the piston ring lubrication with a new boundary condition, *Tribology International,* 31 (1998) 753-760.
[23] J. Choi, S. Lee and S. Park, Friction losses modeling of piston rings for various combustion pressures in diesel engine, *Journal of Mechanical Science and Technology,* 30 (2016) 5739-5747.
[24] L. Zhou, M. Bai and G. Sun, 3D heat transfer, lubrication and friction coupled study for piston ring-liner on diesel engines, *Journal of Mechanical Science and Technology,* 33 (2019) 939-953.
[25] J. F. Booker, Dynamically loaded journal bearings: Mobility method of solution, *Journal of Basic Engineering,* 87 (1965) 537-546.
[26] H. Hirani, K. Athre and S. Biswas, Dynamically loaded finite length journal bearings: Analytical method of solution, *Journal of Tribology,* 121 (1999) 844-852.
[27] Z. P. Mourelatos, An efficient journal bearing lubrication analysis for engine crankshafts, *Tribology Transactions,* 44 (2001) 351-358.
[28] A. Singh, A friction prediction model for small SI engines, *Master's Thesis*, Missouri Univ. of Science and Technology (2013).
[29] R. S. Paranjpe and A. Cusenza, FLARE: An integrated software package for friction and lubrication analysis of automotive engines - Part II: Experimental validation, *SAE International* (1992).
[30] O. P. Taylor, R. Pearson, R. Stone, P. Carden and H. Ballard, Tribological behavior of low viscosity lubricants in the piston to bore zone of a modern spark ignition engine, *SAE Technical Paper* (2014) 1.
[31] J. A. Greenwood and J. H. Tripp, The contact of two nominally flat rough surfaces, *Proceedings of the Institution of Mechanical Engineers,* 185 (1970-1971) 625-633.
[32] Y. Hu, H. S. Cheng, T. Arai, Y. Kobayashi and S. Aoyama, Numerical simulation of piston ring in mixed lubrication—A nonaxisymmetrical analysis, *Journal of Tribology,* 116 (1994) 470.
[33] S. Furuhama, M. Hiruma and M. Tsuzita, *Piston Ring Motion and its Influence on Engine Tribology*, SAE International (1979).
[34] M. Namazian and J. B. Heywood, *Flow in the Piston-cylinder-ring Crevices of a Spark-ignition Engine: Effect on Hydrocarbon Emissions, Efficiency and Power*, SAE International (1982).
[35] R. Keribar, Z. Dursunkaya and M. F. Flemming, An integrated model of ring pack performance, *Journal of Engineering for Gas Turbines and Power,* 113 (1991) 382-389.
[36] M.-R. Cho, D.-Y. Oh, S.-H. Ryu and D.-C. Han, Load characteristics of engine main bearing: Comparison between theory and experiment, *Journal of Mechanical Science and Technol-*

ogy, 16 (2002) 1095-1101.
[37] M. Organisciak, P. Baart, S. Barbera, A. Paykin and M. Schweig, Theoretical and experimental study of the frictional losses of radial shaft seals for industrial gearbox, *Power Transmission Engineering* (2015).
[38] E. Andablo-Reyes, R. Hidalgo-Alvarez and J. de Vicente, Controlling friction using magnetic nanofluids, *Soft Matter*, 7 (2011) 880-883.
[39] C. Bovington, S. Korcek and J. Sorab, The importance of the stribeck curve in the minimisation of engine friction, D. Dowson et al. (editors), *Tribology Series*, 36 (1999) 205-214.
[40] R. A. Mufti and M. Priest, Experimental evaluation of piston-assembly friction under motored and fired conditions in a gasoline engine, *Journal of Tribology,* 127 (2005) 826-836.
[41] R. A. Mufti, Total and component friction in a motored and firing engine, *Doctorial Thesis*, University of Leeds (2004).
[42] W. W. F. Chong, M. Teodorescu and N. D. Vaughan, Cavitation induced starvation for piston-ring/liner tribological conjunction, *Tribology International,* 44 (2011) 483-497.
[43] J. R. Sylvester, Characterization and modeling of rubbing friction in a motored four-cylinder internal combustion engine, *Master's Thesis*, McMaster Univ. (2012).
[44] F. M. Meng, Y. Y. Zhang, Y. Z. Hu and H. Wang, Thermo-elasto-hydrodynamic lubrication analysis of piston skirt considering oil film inertia effect, *Tribology International,* 40 (2007) 1089-1099.
[45] A. Dhar, A. K. Agarwal and V. Saxena, Measurement of dynamic lubricating oil film thickness between piston ring and liner in a motored engine, *Sensors and Actuators A: Physical,* 149 (2009) 7-15.
[46] Q. Xin, Friction and lubrication in diesel engine system design, *Diesel Engine System Design* (2013) 651-758.
[47] P. J. Shayler, W. S. Baylis and M. Murphy, Main bearing friction and thermal interaction during the early seconds of cold engine operation, *Journal of Engineering for Gas Turbines and Power,* 127(2005) 197-205.
[48] R. T. G. Guilherme and S. de Oliveira, Engine oil temperature estimation as an example of a virtual sensor application, *SAE Technical Paper* (2007).
[49] S. Bair, J. Jarzynski and W. O. Winer, The temperature, pressure and time dependence of lubricant viscosity, *Tribology International,* 34 (2001) 461-468.

Seokhwon Lee received his Ph.D. degree from the Department of Convergence of Mechanical Engineering, Hanyang University in 2019. His research interests are the engine friction reduction related to oil lubrication in piston assembly, and bearing.

Jongdae Kang received his B.S. degree from the Department of Mechanical Engineering, Hanyang University in 2017. He is currently in a unified master & Ph.D. course. His research interests are the engine friction analysis.